Wear 270 (2011) 172–180

Contents lists available at ScienceDirect

Wear

journal homepage: www.elsevier.com/locate/wear

Analyses and experimental confirmation of removal performance of silicon oxide film in the chemical–mechanical polishing (CMP) process with pattern geometry of concentric groove pads

Chin-Chung Wei[a,*], Jeng-Haur Horng[a], An-Chen Lee[b], Jen-Fin Lin[c]

[a] Department of Power Mechanical Engineering, National Formosa University, Yunlin, Taiwan
[b] Department of Mechanical Engineering, National Chiao Tung University, Shinchu, Taiwan
[c] Department of Mechanical Engineering, National Cheng Kung University, Tainan, Taiwan

ARTICLE INFO

Article history:
Received 29 March 2010
Received in revised form 3 September 2010
Accepted 20 October 2010
Available online 26 October 2010

Keywords:
Chemical–mechanical polishing
Surface topography
Wear model
Three-body abrasion
Removal rate

ABSTRACT

A Reynolds equation that considers both the smoothing hydrodynamic pressure and the pattern of surface topography at the polishing pads was used to solve the distribution of the hydrodynamic field. A three-body abrasion wear model for solving the removed thickness of silicon oxide films was also introduced to obtain the removal rate of SiO_2 film in a chemical–mechanical polishing (CMP) process. The suction hydrodynamic pressure field expands its region with increasing groove width and decreasing depth of grooves. The flow rate of the slurry was thus increased, and the removal rate also increased with an increased number of abrasive particles. The solid contact pressure was much higher than the hydrodynamic pressure. The three-body abrasion for the wear depth of a particle arises from the solid contacting pressure and is hence more important than the hydrodynamic pressure. The removal rate of the SiO_2 film was dominated by the number of abrasive particles, which was affected by the variation of the hydrodynamic pressure in addition to the wear depth controlled by the solid contact pressure. The thickness of the silicon oxide films removed increased with decreasing grooving width and depth.

1. Introduction

The chemical–mechanical polishing process (CMP) is a key technology in the semiconductor industry. A material, like silicon oxide, is etched by using chemicals and then polished using a mechanical process until it has a smooth and uniform surface. The removal rate and uniformity are important properties that vary with several processing factors. These factors can be separated into three categories: (i) operation conditions, including down force and rotation speeds of the wafer and polishing pad; (ii) properties of the slurry, including pH and the viscosity, size, and shape of wear particles; (iii) properties of the polishing pads, including pattern, asperities, and mechanical properties. The earliest study on the removal rate introduced Preston's equation, $R = KP|V|$ [1], where R is the removal rate, P is the down force, $|V|$ is the absolute value of relative speed between a polishing pad and a wafer, and K is a constant. In this equation, the removal rate is a function of the down force and relative speed; the chemical and fluid effects are not considered. Many studies used this model to find the relationship between the removal rate and operating conditions. McFarlane and Tabor [2] discussed the influence of the adhesion effect of wear particles on the real contact area. Eringen [3] added the micro spinning effect of wear particles and the stress couple effect of the flow field to the micro-fluid analysis. Cook [4] replaced the pressure and velocity parts of Preston's equation with the normal and shear stresses to find more correct results for the removal rate. Runnels and Eyman [5], Runnels [6], and Sundararajan et al. [7] studied the lubrication parameters and wear rate of the CMP process by solving the Navier–Stokes equation or the Reynolds equation. This approach assumes slurry erosion to be responsible for the wear mechanism and neglects abrasion wear by particles entrapped in the surface of the polishing pad. The study of Seok et al. [8] described a multistage model for material removal. This model is based on the deformation of hyper-elastic asperities attached to a linear-elastic pad. Zhao and Chang [9] developed a model based on the elastic–plastic micro-contact mechanics and abrasive wear theory. The synergetic effects of mechanical and chemical actions are included in the model. The model reveals some insights into the microcontact and wear mechanisms of the CMP process. Yu et al. [10,11], Murarka and Gutmann [12], and Lee et al. [13] established microcontact models and analysed the contact behaviour between the polishing pad and wafer with viscous-elastic and plastic contact models at two rough contacting surfaces. Tichy et al. [14] presented a one-dimensional model to predict the magnitude of measured

* Corresponding author. Tel.: +886 56315414; fax: +886 56312110.
E-mail address: ccwei@nfu.edu.tw (C.-C. Wei).

0043-1648/$ – see front matter © 2010 Elsevier B.V. All rights reserved.
doi:10.1016/j.wear.2010.10.057

Nomenclature

F_B	back force applied by the wafer carrier (N)
F_C	contact force (N)
F_D	down force (N)
F_L	hydrodynamic force (N)
M_g	wafer weight (N)
P_B	back pressure applied from the wafer carrier (Pa)
P_c	solid contact pressure (Pa)
P_L	hydrodynamic pressure (Pa)
ϕ	attack angle (rad)
ψ, θ	spinning angles of wafer and pad, respectively (rad)
R_C	diameter of wafer (m)
ω_p, ω_c	wafer and polishing pad angular speeds, respectively (rpm)
P	hydrodynamic pressure between two contact surfaces (Pa)
r, θ	cylindrical coordinates
Φ_r, Φ_θ,	flow factors along the r and θ directions, respectively
Φ_{Sr}	shear flow factor in the r direction
μ	viscous of slurry
γ	coefficient of roughness of patterns
h_{rd}, h_g	film thickness in and away from groove area
u_{1r}, u_{2r}, $u_{1\theta}$, $u_{2\theta}$	flow velocities along the r,θ directions at upper (subscript 1) and lower (subscript 2) surfaces, respectively (m/s)
R_d	distance between the centres of the wafer and polishing pad (m)
α, β	flow rates along the r and θ directions, respectively
P_{WP}	pressure produced by the contact load of a solid applied at the real contact area (Pa)
A_{WP}	circular contact area of roughness peaks (m^2)
δ	deformation of roughness peaks (m)
E_{WP}	effective elastic modulus (Pa)
E_W, E_p, E_A	modulus of a wafer polishing pad, and particle of slurry, respectively (Pa)
ν_W, ν_p, ν_A	Poisson's ratio of a wafer polishing pad, and particle of slurry, respectively
R_p	curvature radius of the roughness peaks on a polishing pad (m)
$\phi(z_s)$	Gaussian probability density function
a_{WP}	contract radius of roughness peak (m)
δ_c	critical yielding deformation (m)
H_W	surface hardness of a wafer (Pa)
A_{WAe}, A_{WAp}	real elastic and plastic contact areas formed at the wear particle and wafer contact region, respectively (m^2)
R_{WA}	complex curvature radii of contact roughness peaks existing at two contact surfaces (m)
R_W, R_A	curvature radii of roughness peaks on a wafer and a pad, respectively
F_{WAe}, F_{WAp}	contact loads created by elastic and plastic contact, respectively (N)
h_a	contact distance between the surface of a wafer and a wear particle (m)
$\phi(z_a)$	probability density function of roughness peaks on a pad along the altitude direction
F_{WA}	contact load created by a wear particle acting on a wafer (N)
P_{WA}	real contact pressure of a wear particle (Pa)
A_{WA}	projection area of a wear particle (m^2)
δ_{aw}	deformation created between the particle and wafer (m)
δ_{ap}	deformation created between the particle and pad (m)
V	relative sliding speed at two contact surfaces (m/s)
t	process time (s)
k	wear constant
r	contact radius of contact roughness (m)
n_a	concentration of particles of slurry (numbers/m^3)
ε_0	factor of chemical reaction

sub-ambient hydrodynamic pressure in the CMP process. The formation of a subambient hydrodynamic pressure region in part of the wafer lubrication area was found in the experimental results of Shan et al. [15] and Levert et al. [16]. An abrasive mechanism in solid–solid contact model was investigated in the model studied by Luo and Dornfeld [17]. This model developed for material removal considered the concentration of active abrasives in the slurry. The proposed model integrates the process parameters including pressure, velocity, and other important input parameters. The effects of particles size were investigated in the study of Jeng and Huang [18]. They proposed a CMP removal rate model based upon a micro-contact model which considered the effects of the abrasive particles located between the polishing interfaces. The roughness factor of the polishing pad and the wear particles in the CMP fluid analysis model have been extensively discussed by Thakurtaa et al. [19], Vlassak et al. [20], Qin et al. [21] and Wei et al. [22]. In this study, the model developed by Luo and Dornfeld [17] for the number of active abrasive particles was improved, and a micro-contact model was included. High subambient pressures are liable to generate in the use of a non-grooved pad. Therefore, a large suction force is formed between the wafer and the pad such that they are often difficult to separate from each other. The feasible way of lowering the subambient pressure is the applications of different groove patterns in the pad. In many engineering applications, surfaces are grooved into different patterns to enhance friction and lubrication performance. Lloy [23] reported that the patterns of grooves in wet clutch surfaces affect the drag loss during the disengaged state. Razzzaque and Kato [24] observed similar results in their experiments and attempted to incorporate grooving effects in squeeze film analysis. In the studies of Berger et al. [25] the groove effect in an engagement model was introduced in their analysis; however, only a small number of radial grooves were considered. Various patterns and shapes of polishing pad grooves can increase the removal rate and uniformity of wafers. Lin et al. studied analysis models of the slurry fluid field by using concentric and spot patterns of polishing pads [26,27]. They solved CMP problem by developing the average Reynolds equation with flow factors to study the mixed lubrication arising at a cylindrical coordinate system. A theoretical abrasive and adhesive wear model was developed to evaluate the removal rate of the copper film. Subambient hydrodynamic pressure was predicted to be formed in part of the wafer's lubrication area.

The present work extends the analyses of the CMP fluid field of Lin et al. [27] with a three body micro-contact model [28] to improve the model, and a well removal analysis is also introduced in the fluid analysing model. The removal rate and uniformity of wafers were found for several widths and depths of grooves in concentric pattern pads. These analysis results were also confirmed with experimental data obtained from an industrial CMP device. A referenced tendency of pressure distribution of fluid field in the geometric design of concentric patterns of a CMP pad is also provided to find the better design coefficients for removal rate and god uniformity of SiO_2 film.

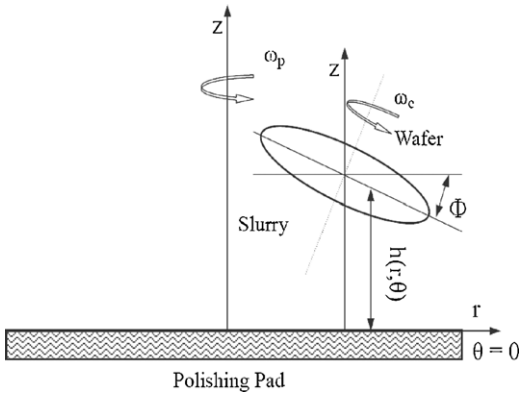

Fig. 1. A sketch of a wafer and polishing pad at steady state.

2. Analysing the model and experiment

The hydrodynamic pressure of a slurry is formed between a wafer and polishing pad with a small angle of inclination between the wafer and polishing pad during the CMP process, which is called the attack angle, ϕ, as shown in Fig. 1. This angle leads to hydrodynamic pressure at the contact surface and allows the slurry to flow smoothly into the gap between the pad and wafer. The attack angle cannot be directly controlled; it depends on the kinematical balance of the CMP device, including force and moment equilibriums. Equivalent equations obtained from the forces are [27]:

$$-F_B - F_D - M_g \cos\phi + F_L + F_C = 0 \tag{1}$$

where M_g is the weight of a wafer, F_B is the back force applied by the wafer carrier, F_D is the down force, F_L is the hydrodynamic force, and F_C is a contact force. The equivalent equations for the moments are [27]:

$$\begin{aligned}(M_{x'})_{\text{total}} = &\int_0^{2\pi}\int_0^{R_C} p_L(r,\theta) r^2 \cos(\psi-\theta)\, dr d\theta \\ &+ \int_0^{2\pi}\int_0^{R_C} p_c(r,\theta) r^2 \cos(\psi-\theta)\, dr d\theta \\ &- \sum_{i=1}^{N} r_i p_B A_B \cos(\psi-\theta_i) = 0\end{aligned} \tag{2}$$

$$\begin{aligned}(M_{y'})_{\text{total}} = &\int_0^{2\pi}\int_0^{R_C} p_L(r,\theta) r^2 \sin(\psi-\theta)\, dr d\theta \\ &+ \int_0^{2\pi}\int_0^{R_C} p_c(r,\theta) r^2 \sin(\psi-\theta)\, dr d\theta \\ &- \sum_{i=1}^{N} r_i p_B A_B \sin(\psi-\theta_i) = 0\end{aligned} \tag{3}$$

where P_L is the hydrodynamic pressure, P_c is the solid contact pressure, P_B is the back pressure applied by the wafer carrier, R_c is diameter of the wafer, and ψ and θ are the spinning angles of the wafer and pad, respectively. Eqs. (1)–(3) were used to calculate the minimum film thickness, its position, and the attack angle, which were then used as the initial values in the flow field model. Two cylindrical coordinates were used to describe the motions of the wafer and polishing pad, as shown in Fig. 2. The wafer and polishing pad were rotated with angular speeds ω_p and ω_c, respectively, in the counter-clockwise direction.

The depth of the groove is much greater than the surface roughness. The surface asperities can thus be ignored on the polishing pad in the region with grooves. The roughness effect in the flow field model is still considered for the region without grooves. From Lin et al. [27], a Reynolds equation that considers both the smoothing hydrodynamic pressure and the pattern effect at the polishing pads is:

$$\begin{aligned}\frac{\partial}{\partial r}\left[H_1\left(\frac{\partial p}{\partial r}\right) + H_2\left(\frac{1}{r}\frac{\partial p}{\partial \theta}\right)\right] + \frac{\partial}{\partial \theta}\left[H_3\left(\frac{\partial p}{\partial r}\right) + H_4\left(\frac{1}{r}\frac{\partial p}{\partial \theta}\right)\right] \\ = \frac{\partial}{\partial r}(F_1) + \frac{\partial}{\partial \theta}(F_2)\end{aligned} \tag{4}$$

where

$$H_1 = \frac{r\Phi_r f(N,e,h_{rd})}{12\mu}\frac{h_\alpha + h_\beta - \beta h_\alpha - \beta h_{rd}^3}{h_\alpha + h_\beta} + \frac{r\beta f(N,e,h_g)}{12\mu}\frac{h_\alpha + h_{rd}^3}{h_\alpha + h_\beta} \tag{5a}$$

$$H_2 = \frac{r\Phi_r f(N,e,h_{rd})}{12\mu}\frac{1-\beta}{1-\alpha}\beta\tan\gamma\frac{h_\alpha - h_{rd}^3}{h_\alpha + h_\beta} + \frac{r\beta f(N,e,h_g)}{12\mu}\frac{1-\beta}{1-\alpha}\tan\gamma\frac{h_\alpha - h_{rd}^3}{h_\alpha + h_\beta} \tag{5b}$$

$$H_3 = -\frac{\Phi_\theta f(N,e,h_{rd})}{12\mu}\frac{1-\alpha}{1-\beta}\alpha\cot\gamma\frac{h_\beta - h_{rd}^3}{h_\alpha + h_\beta} + \frac{f(N,e,h_g)}{12\mu}\frac{1-\alpha}{1-\beta}\alpha\cot\gamma\frac{h_\beta - h_{rd}^3}{h_\alpha + h_\beta} \tag{5c}$$

$$H_4 = -\frac{\Phi_\theta f(N,e,h_{rd})}{12\mu}\frac{h_\alpha + h_\beta - \alpha h_\beta - \alpha h_{rd}^3}{h_\alpha + h_\beta} + \frac{f(N,e,h_g)}{12\mu}\alpha\frac{h_\beta + h_{rd}^3}{h_\alpha + h_\beta} \tag{5d}$$

$$\begin{aligned}F_1 = &\, r(1-\beta)\left(\frac{\tilde{h}_{Trd}}{2}(u_{1r}+u_{2r}) + \frac{\sigma}{2}(u_{1r}-u_{2r})\frac{\partial \Phi_{sr}}{\partial r}\right) + r\beta\frac{h_g}{2}(u_{1r}+u_{2r}) \\ &- \frac{r\Phi_r f(N,e,h_{rd})}{12\mu}\beta(1-\beta)\tan\gamma\frac{m}{h_\alpha + h_\beta} + \frac{rf(N,e,h_g)}{12\mu}\beta(1-\beta)\tan\gamma\frac{m}{h_\alpha + h_\beta}\end{aligned} \tag{5e}$$

$$\begin{aligned}F_2 = &\,(1-\alpha)\left(\frac{\tilde{h}_{Trd}}{2}(u_{1\theta}+u_{2\theta}) + \frac{\sigma}{2}(u_{1\theta}-u_{2\theta})\frac{\partial \Phi_{sr}}{\partial \theta}\right) + \alpha\frac{h_g}{2}(u_{1\theta}+u_{2\theta}) \\ &+ \frac{\Phi_\theta f(N,e,h_{rd})}{12\mu}\alpha(1-\alpha)\frac{m}{h_\alpha + h_\beta} - \frac{f(N,e,h_g)}{12\mu}\alpha(1-\alpha)\frac{m}{h_\alpha + h_\beta}\end{aligned} \tag{5f}$$

where the coefficients h_α, h_β, and m and the function $f(N, e, h_{rd})$ are written as:

$$h_\alpha = (1-\alpha)h_g^3 + (\alpha)h_{rd}^3 \tag{6a}$$

$$h_\beta = (1-\beta)h_g^3 + \beta h_{rd}^3 \tag{6b}$$

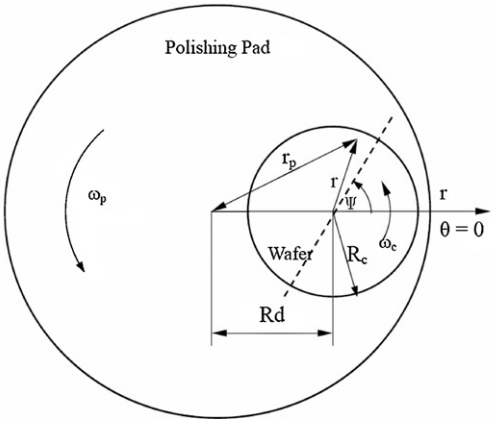

Fig. 2. Coordinates of a wafer and a pad.

$$m = [-6r\omega_c(h_g + h_{rd}) - 6\omega_p(r + R_d\cos\theta)(h_g + h_{rd})] + 6(h_g + h_{rd})R_d\omega_p \sin\theta\cot\gamma \quad (6c)$$

$$f(N, e, h_{rd}) = h_{rd}^3 + 12e^2h_{rd} - 6Neh_T^2\,Coth\left(\frac{Nh_{rd}}{2e}\right) \quad (6d)$$

Here, P is the hydrodynamic pressure formed between the wafer and polishing pad, r and θ are the cylindrical coordinates, Φ_r and Φ_θ are flow factors along the r and θ directions, respectively, Φ_{Sr} is the shear flow factor in the r direction, μ is the viscous of slurry, and γ is the parameter of the roughness patterns. $\gamma = \lambda_{0.5r}/\lambda_{0.5\theta}\cdot\lambda_{0.5r}$ and $\lambda_{0.5\theta}$ are the self-correlation functions of the surface asperities along the r and θ directions, respectively. h_g and h_{rd} are the film thicknesses at the regions with and without grooves, respectively. $u_{1r}, u_{2r}, u_{1\theta}$, and $u_{2\theta}$ are the flow velocities along the r,θ directions at upper and lower surfaces, respectively. R_d is the distance between the centres of the wafer and polishing pad. α and β are flow rates along the r and θ directions, respectively; they were assumed to be equal. The boundary equation was given as follows: when the radius from the centre of the wafer, r, is equal to the radius of the wafer, R_c, the hydrodynamic pressure is equal to the atmosphere pressure (1 atm). Based on Eq. (1), the hydrodynamic pressure can be obtained using the finite difference method. The fluid velocity and the flow rate at any position in the flow field can be obtained by using the gradient of the hydrodynamic pressure and the boundary velocity.

The deformation of a polishing pad was assumed under the elastic limit. The contact pressure produced by the roughness of pads can thus be obtained by the elastic contact theory as [28]:

$$P_{WP} = \frac{4}{3}\frac{E_{WP}}{\pi(R_P)^{1/2}}\int_h^\infty (z_s - h)^{1/2}\cdot\phi(z_s)\,dz_s \quad (7)$$

where P_{WP} is the pressure produced by the contact load of a solid applied at the real contact area, A_{WP}. δ is the compressible deformation of the roughness peaks, $\delta = z_s - h$. E_{WP} is the effective elastic modulus:

$$E_{WP} = \left(\frac{1-\nu_W^2}{E_W} + \frac{1-\nu_P^2}{E_P}\right)^{-1} \quad (8)$$

where E_W and ν_W are the modulus and the Poisson's ratio of the polished surface of the wafer, respectively. E_p and ν_p are the modulus and the Poisson's ratio of the roughness peaks on the polishing pad, respectively. R_p is the radius of curvature of the roughness peaks on a polishing pad, and $\phi(z_s)$ is the Gaussian probability density function.

$$\phi(z_s) = \frac{1}{\sigma\sqrt{2\pi}}\exp\left(-\frac{z_s^2}{2\sigma^2}\right) \quad (9)$$

The contact radius of the surface roughness produced by the pad and wafer, a_{WP}, is:

$$a_{WP} = (R_P)^{1/2}(\delta)^{1/2} \quad (10)$$

An elastro-plastic model was used to simulate wear particles contacting the wafer surface. Several assumptions were used to modify the behaviour of the wear particles. (1) Wear particles were distributed uniformly on the wafer and polishing pad; a surface roughness that consists of wear particles was homogeneous and independent of time. (2) The Gaussian distribution function was used to describe the distribution of wear particles on roughness peaks. (3) The contact behaviour of the roughness peaks between the wafer and pad was elastro-plastic contact. (4) The radii of curvature of the roughness peaks on the pad were assumed to be equal. (5) The roughness peaks were independent of each other. (6) The hydrodynamic pressure and fluid film did not exist in the contact region. The Hertz contact theory was used to describe the contact behaviour of the roughness peaks [28]. Tabor [29] showed that for the elastic deformation formed at all roughness peaks of two roughness plates, the average contact stress was $P_m = K_cH$, where H is the hardness of the softer material and K_c is a constant. The critical yielding deformation, δ_c, can be written as:

$$\delta_c = \left(\frac{\pi K_c H_W}{2E_{WA}}\right)^2 R_{WA} \quad (11)$$

E_A and ν_A are the elastic modulus and the Poisson's ratio of the wear particles, respectively. H_W is the hardness of the wafer on the polishing side. The real contact area formed by a particle in contact with a wafer surface can be written as [30]:

$$\begin{aligned} A_{WA}(h_a) &= A_{WAe}(h_a) + A_{WAp}(h_a) \\ &= \pi R_{WA}\int_{h_a}^{h_a+\delta_c}(z_a - h_a)\phi_w(z_a)\,dz_a \\ &\quad + \pi R_{WA}\int_{h_a+\delta_c}^{\infty}\phi_w(2(z_a - h_a) - \delta_c)(z_a)\,dz_a \end{aligned} \quad (12)$$

where $A_{WAe}(h_a)$ and $A_{WAp}(h_a)$ are the real elastic and plastic contact areas formed at the wear particle and wafer contact regions, respectively. R_{WA} is the complex radius of curvature of the roughness peaks and is written as:

$$R_{WA} = \left(\frac{1}{R_W} + \frac{1}{R_A}\right)^{-1} \quad (13)$$

where R_W and R_A are the radii of curvature of the roughness peaks on the wafer and pad, respectively. The value of R_A is half of the secondary particle size. The elastro-plastic contact load of a wear particle is written as:

$$\begin{aligned} F_{WA}(h_a) &= F_{WAe}(h_a) + F_{WAp}(h_a) \\ &= \frac{4}{3}E_{WA}R_{WA}^{0.5}\int_{h_a}^{h_a+\delta_c}(z_a - h_a)^{1.5}\phi(z_a)\,dz_a \\ &\quad + \pi K_c H_W R_{WA}\int_{h_a+\delta_c}^{\infty}(2(z_a - h_a) - \delta_c)\phi(z_a)\,dz_a \end{aligned} \quad (14)$$

where $F_{WAe}(h_a)$ and $F_{WAp}(h_a)$ are the contact loads created by elastic and plastic contact, respectively, which act on the real contact area between the wafer and pad. h_a is the distance from the surface of a wear particle to the wafer. $\phi(z_a)$ is the probability density function of roughness peaks on a pad along the altitude direction.

The contact load created by a wear particle acting on the wafer, denoted as F_{WA}, can be obtained by the contact pressure, P_{WA}, created by the contact between the wafer and pad, and the projection area of a wear particle, A_{WA}. F_{WA} can thus be written as:

$$F_{WA} = P_{WA}A_{WA} = P_{WA}\pi(R_A)^2 \quad (15)$$

From this equation, the real contact pressure of a wear particle, P_{WA}, can thus be written as:

$$P_{WA} = \frac{F_{WA}}{A_{WA}} = \frac{F_{WA}}{\pi(R_A)^2} \quad (16)$$

The removal rate of wafers, RR, is usually defined as the average removed thickness per unit time. Fig. 3 shows a wear particle acting on a flat plate. x is the contact length of the particle and specimen. δ_{aw} is the deformation created by the particle and wafer. δ_{ap} is the deformation created by the particle and pad when the removal area of a particle at the surface of the wafer, ΔS, is very small. The wear volume of a particle is written as:

$$\Delta\bar{V} = k\,\Delta S V t \approx kVt\delta_{aw}\sqrt{\delta_{aw}x} \quad (17)$$

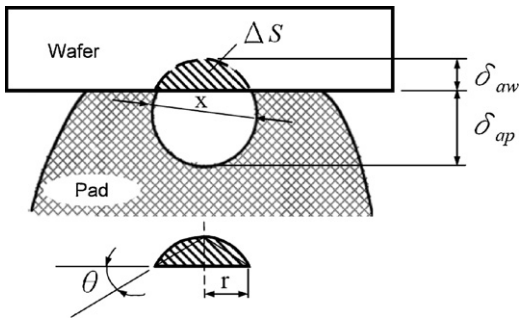

Fig. 3. A sketch of the wear volume of a particle.

where V is the relative sliding speed, t is the wear time, and k is a constant of wear. With the use of Eq. (17), the removal rate is:

$$RR = \frac{\Delta \bar{V} n_a}{A_n t} = \frac{kV\delta_{au}\sqrt{\delta_{au}x}n_a}{A_n} \tag{18}$$

where n_a is the concentration of particles. Xie and Williams [31] introduced the attack angle, θ, formed between a particle and wafer as shown in Fig. 3, which affects the wear volume. When the attack angle, θ, is less than 15°, and the pressed depth of a wear particle is assumed to be very small compared to the diameter of a particle, the wear constant k can be written as:

$$k \approx \frac{3}{\pi}\sqrt{\frac{\delta_{aw}}{x}} \tag{19}$$

The removal rate can be rewritten as [30]:

$$RR = \frac{3\varepsilon_0 V\delta_{aw}^2}{\pi A_n}\eta_a A_{ud}\int_{X_{\max}-\delta_{ap}}^{X_{\max}} \phi_a(x)\,dx \tag{20}$$

where η_a is the number of particles of contact area. $\phi_a(x)$ is the Gauss density function. ε_0 is introduced as a chemical factor in the removal rate function, RR. If the chemical factor $\varepsilon_0 = 1$, which means that non-chemical effect occurring at the contact area.

3. Results and discussion

The numerical calculation flow chart is shown in Fig. 4. The force and moment equations were used to solve for the minimum slurry film thickness, spinning angle φ, and attack angle ϕ as initial conditions. The Reynold's equation, considering both the smoothing hydrodynamic pressure and the pattern of the pad, was solved to obtain the hydrodynamic pressure distribution, and the solid contact pressure was used to obtain the applied normal load. Then the force balance equation was iterated until it converged. The wear theory of particles was then used to obtain the distribution of the removal rate of the silicon oxide film, which varied with the pattern of concentric pads in the radial direction. All coefficients of the material and the operating conditions are shown in detail in Tables 1 and 2, respectively. In the analysis model, several parameters were obtained from experimental measurements, including the hardness of the wafer and pad and particle size and concentration in the slurry. The experiment was conducted on a commercial CMP device. The rotational speed of the pad and wafer carrier was 90 rpm counter-clockwise. The down force was 1 psi, or about 6.896 kPa. The polishing duration time for each wafer was 40 s. Because slurry filled in the clearance between the wafer and pad, the fluid behaviour of slurry in this gap between the wafer and pad can be considered as a fully developed flow.

Many factors affect the removal rate and uniformity of the silicon oxide film treated by the CMP process. A new theoretical model was established and presented to analyse the fluid field, removal rate and uniformity, which varied with the groove depth and width

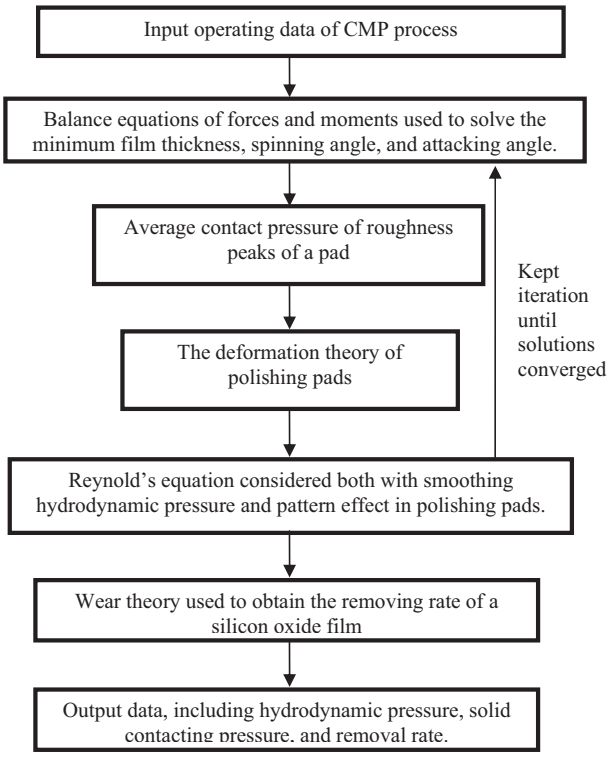

Fig. 4. Flow chart of the CMP model.

Table 1
The material properties and conditions used in the numerical calculation.

Nanohardness of the SiO_2 film wafer without a passivation layer, E_w (GPa)	10.88
Young's modulus of the SiO_2 film wafer without a passivation layer, E_w (GPa)	72.4
Poisson's ratio of the SiO_2 film, ν_w	0.2
Young's modulus of abrasive particles (Al_2O_3), E_a (GPa)	393
Poisson ratio of abrasive particles (Al_2O_3), ν_a (GPa)	0.27
Mean radius of abrasive particles (Al_2O_3), R_a (μm)	0.2
Young's modulus of pad's asperities, E_p (MPa)	100
Poisson ratio of pad's asperities and substrate, ν_p and ν_{ps}	0.3
Young's modulus of pad's substrate, E_{ps} (MPa)	2.4
Viscosity of the slurry (Ns/m^2)	0.001
Standard deviation of pad's roughness heights (μm)	15
Mean radius of curvature for pad's roughness heights, R_p (μm)	50
Pad's asperity density, η_s (1/m^2)	4.3×10^7
Distance between the centres of wafer and pad, Rd (m)	0.6096
Wafer radius, R_c (m)	0.3048
Density of the slurry before dilution, ρ_s (g/mm^3)	1×10^{-3}
Density of abrasives, ρ_a (g/mm^3)	4×10^{-3}
Average volume of a single abrasive, $\bar{V}_a$ (μm^3)	1.4×10^{-2}
Mean height of a single asperity, l (m)	1.5×10^{-5}

Table 2
The operation conditions used in the study.

Polishing pad	Rodel Politex Regular E (IC1400)
Down-force pressure	6.896 kPa
Back Pressure	10.34 kPa
Platen speed	90 rpm
Carrier speed	90 rpm
Slurry flow rate	150×10^{-6} m^3/min
Plating temperature	37 °C
Polishing time	40 s
Pre-wet duration	20 s
Pre-wet flow rate	300×10^{-6} m^3/min
Pad condition	Manual brushing

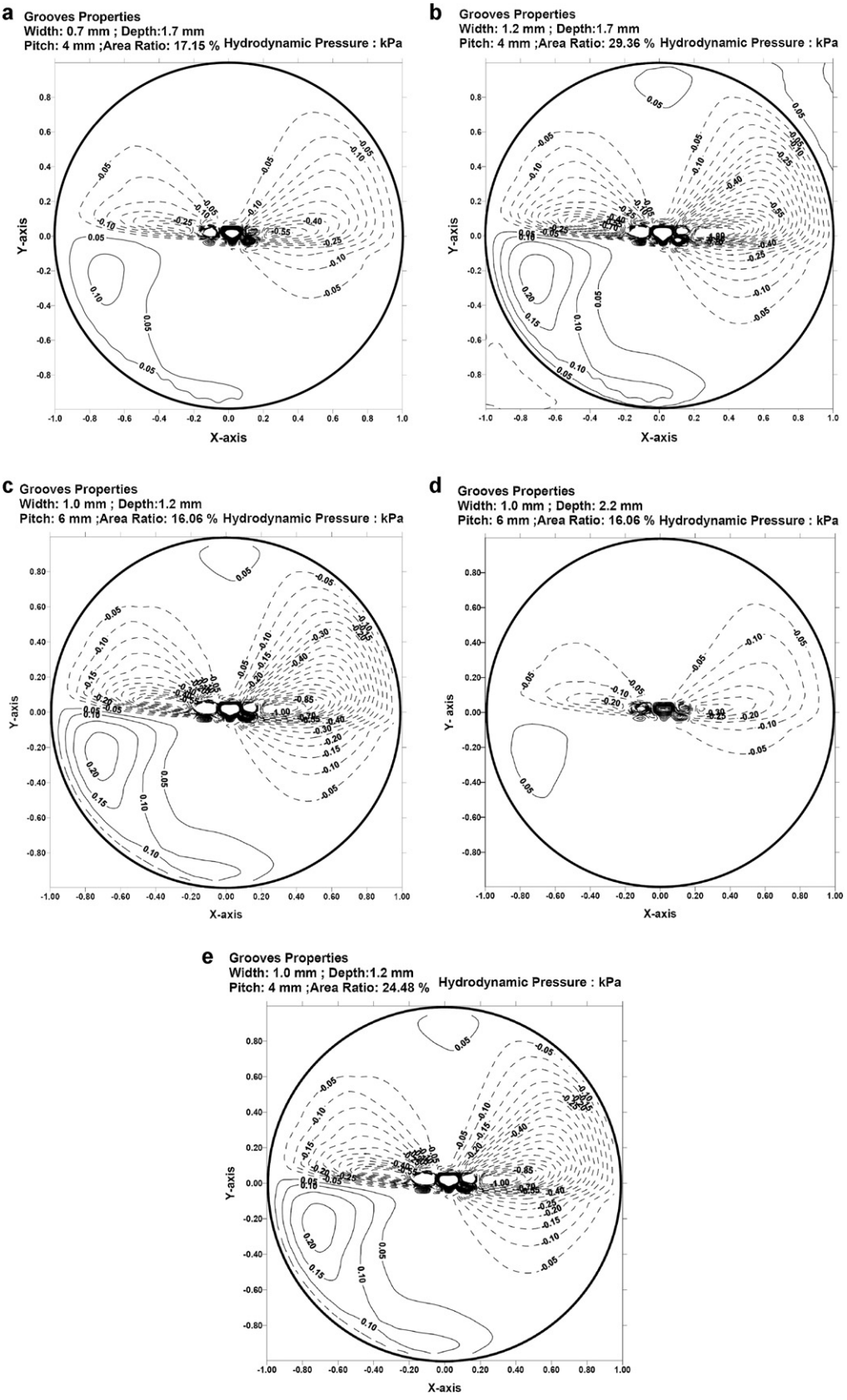

Fig. 5. Contour diagram of hydrodynamic pressure varying with different conditions of concentric grooves on a dimensionless wafer area: (a) width is 0.7 mm, depth is 1.7 mm, groove pitch is 4 mm, and area ratio of grooves on a pad is 17.15%; (b) width is 1.2 mm, depth is 1.7 mm, groove pitch is 4 mm, and area ratio of grooves on a pad is 29.36%; (c) width is 1 mm, depth is 1.2 mm, groove pitch is 6 mm, and area ratio of grooves on a pad is 16.06%; (d) width is 1 mm, depth is 2.3 mm, groove pitch is 6 mm, and area ratio of grooves on a pad is 16.06%; (e) width is 1 mm, depth is 1.2 mm, groove pitch is 4 mm, and area ratio of grooves on a pad is 24.48%.

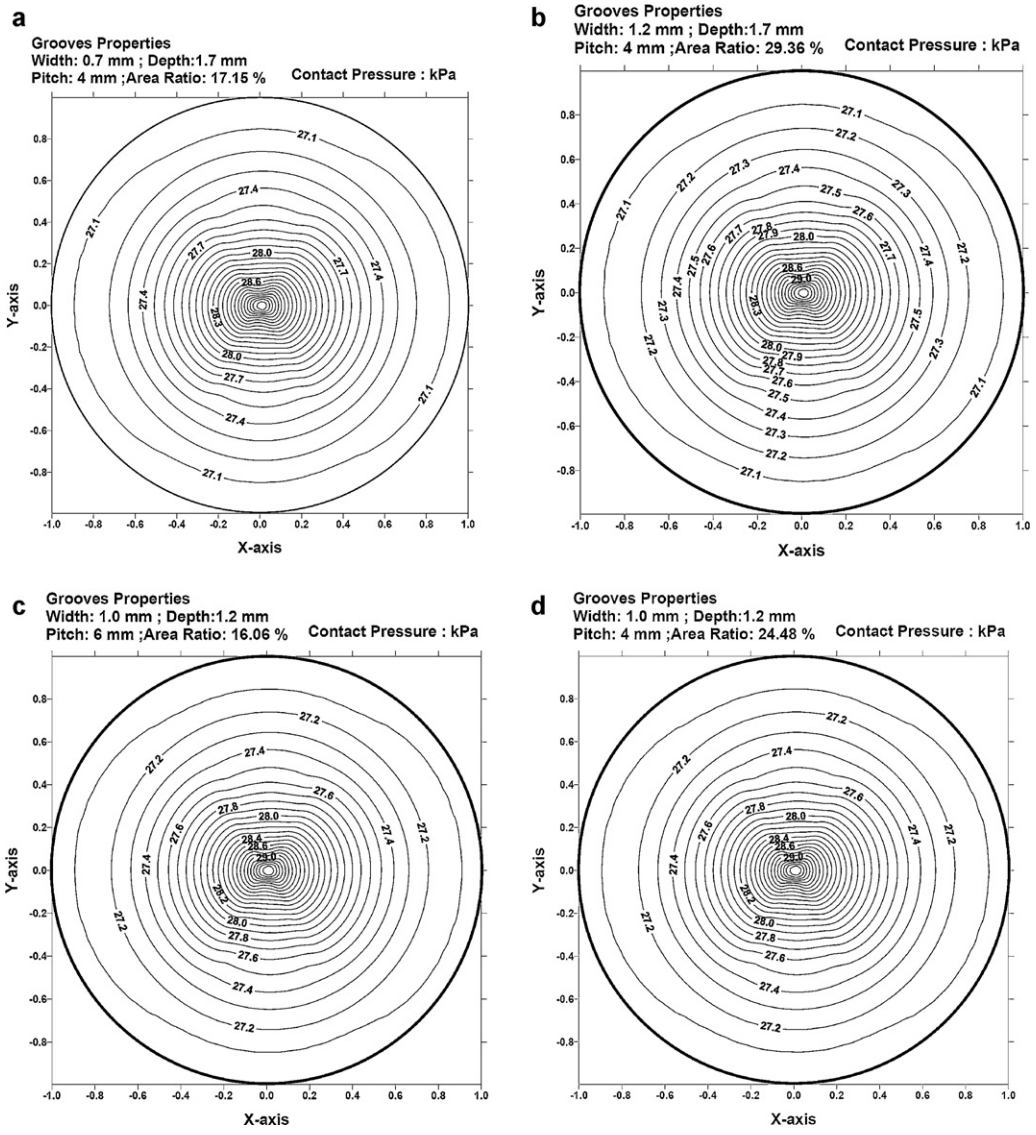

Fig. 6. Contour diagram of solid contact pressure varying with different conditions of concentric grooves on a dimensionless wafer area: (a) width is 0.7 mm, depth is 1.7 mm, groove pitch is 4 mm, and area ratio of grooves on a pad is 17.15%; (b) width is 1.2 mm, depth is 1.7 mm, groove pitch is 4 mm, and area ratio of grooves on a pad is 29.36%; (c) width is 1 mm, depth is 1.2 mm, groove pitch is 6 mm, and area ratio of grooves on a pad is 16.06%; (d) width is 1 mm, depth is 1.2 mm, groove pitch is 4 mm, and area ratio of grooves on a pad is 24.48%.

and the area ratio of the concentric groove pads. The area ratio is the area of the grooves divided by the area of the whole pad. A high area ratio indicates that a higher groove area existed on a pad, the real contact area formed at a wafer and pad. In this study, the removal rate varied with the radii of the wafer according to the theoretical analyses and was confirmed with the experimental data, which provided the correction of the numerical data.

3.1. The hydrodynamic pressure

Particles in slurry move with the flow direction of the fluid field, which varies with the gradient of the hydrodynamic pressure. When the variation of the hydrodynamic pressure is large, the motion of particles is violent, and a good uniformity of a polished wafer can thus be obtained. The distribution of the hydrodynamic pressure formed at the contact area affects the flow direction of the slurry; the number of abrasive particles at the contact area thus varies with it. Fig. 5 shows the contour graphs of hydrodynamic pressures varying with grooving width, depth, pitch, and area ratio. The area ratio of a pad varies with the groove width and the pitch of the grooves. In Fig. 5, the distribution of the hydrodynamic pressure can be separated into negative and positive fields. In the positive pressure field formed at the contact area between the wafer and pad, the fluid pressure forms to separate these two contact surfaces; the slurry can thus flow into the contact area. Otherwise, the negative hydrodynamic pressure, also named the suction pressure, allows these two contact surfaces, that is, the wafer and polishing pad, to be in contact, and thus the abrasive particles can remove material. The polishing behaviour thus occurs mainly at the negative pressure field. Contour lines formed several eddies at and near the centre of the pad; the flow rate of the slurry thus became lower than that in the other area. Neither the negative nor the positive hydrodynamic pressure regions nor the pressure gradient increased with grooves of greater width, as shown in Fig. 5(a) and (b), or shallower depth, as shown in Fig. 5(c) and (d). These phenomena indicate that a narrow groove width means the slurry cannot flow out smoothly. Deeper grooving depth also let the slurry stay at the groove for a longer time instead of flowing out. The slurry thus filled the gap between the wafer and pad, and the suction and positive pressures were hence decreased. Fig. 5(c) and (e) shows that

the hydrodynamic pressure varies with different groove pitches, which vary with the area ratio of the pad. Comparing these two figures, the distributions of the hydrodynamic pressure seem similarly, and the flow of the slurry does not vary significantly with different groove pitches.

3.2. The solid contacting pressure

Fig. 6 shows the distributions of that solid contacting pressures varying with groove width, depth, pitch, and area ratio of the concentric grooved pad on the dimensionless contact area of the wafer. Different groove widths, depths, and pitches only slightly affect the distribution of the solid contacting pressure. However, their values are much higher than the hydrodynamic pressure, as shown in Fig. 5. Because the total pressure applied at the contact area is the sum of the solid contacting pressure and the hydrodynamic pressure, the abrasive effect for the wear depth of a particle due to the solid contacting pressure is hence more important than hydrodynamic pressure. However, the removal rate is also affected by the number of abrasive particles in the slurry, which increases with increasing gradient of hydrodynamic pressure.

3.3. The removal rate and uniformity of SiO_2 film

Fig. 7 shows the removed thickness of the SiO_2 film varying with the dimensionless radius of the wafer area and the geometrical parameters of the polishing pads, including groove width, depth, pitch, and area ratio. Fig. 7(a) and (b) are the groove pitches of 4 mm and 6 mm, respectively. These two figures show that the results of analysis and experiments are well matched, especially in Fig. 7(a). The value of the removed thickness near the centre of the wafer is lower than those at other positions. This is due to the distribution of the hydrodynamic pressure, which forms several eddies near the centre, which let the slurry quickly flow into the area and thus decreases the number of abrasive particles. The removal rate was also affected by the effective density of particles and not only by the wear depth controlled by the solid contacting pressure. The removed thickness of silicon oxide films increased with decreasing width and depth of grooves, as shown in Fig. 7(a) and (b). A narrow groove decreases the area ratio of grooves on a pad and increases the contact area of wear particles. A shallow groove lets more slurry and particles stay on the pad surface, making the slurry flow more violent due to a higher gradient of the hydrodynamic pressure field, as shown in Fig. 5(c) and (d). In the study of Lin et al. [27], the application of concentric grooves in general lowered the suction pressure (negative pressure) formed between the pad and the wafer, elevated the removal rate and reduced the non-uniformity. However, the influences of the groove depth on the removal rate and non-uniformity become insignificant when the depth is excessively large because the operating speed was 35 rpm in the study of Lin et al. [27], but the machine here was operated at 90 rpm, which is twice as high. The distribution of the hydrodynamic pressure analysed at 35 rpm in Lin's study [27] varied more smoothly than that obtained at the speed of 90 rpm, as shown in Fig. 5. They also indicated that the removal rate was reduced by increasing the groove width such that it finally approached the result of a non-grooved pad, which is the same as our findings, as shown in Fig. 7(a) and (b). Several situations were not considered in the proposed model, like the flatness of the polishing pad and the starvation effect without grooves. This may be a result of the assumption that the slurry must fill in the clearance between the wafer and pad. In a wide pitch pad, starvation may decrease the hydrodynamic pressure, but this phenomenon cannot be found in Fig. 5(c) and (e). However, starvation behaviour was not considered in the proposed CMP model, which led to estimation error in the removal rate calculation results. More calculation error can be found in Fig. 7(b). Fig. 7 shows that the optimum conditions of a concentric pad for silicon oxide polishing are a width of 1 mm, a depth of 1.2 mm, and a pitch of 4 mm for a removal rate of 3100 A/min and a non-uniformity of under 5%.

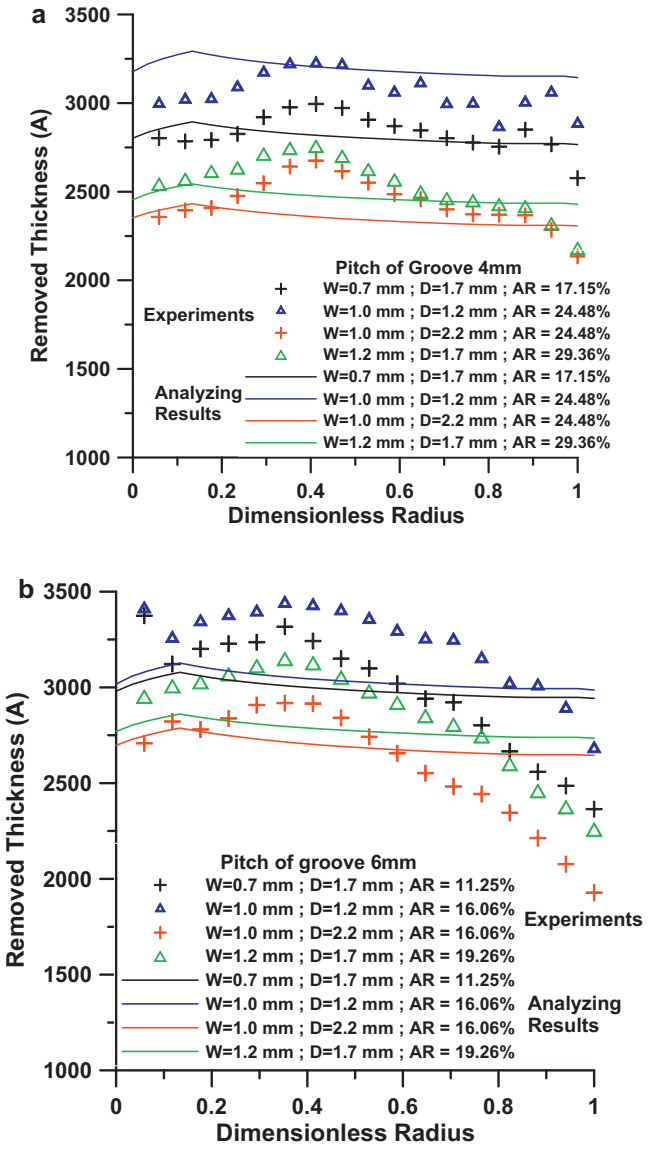

Fig. 7. Removal rates varied with different geometrical conditions of concentric grooves were obtained from experiments and theoretical analyses and comparing with each other: (a) groove pitch is 4 mm, and (b) groove pitch is 6 mm.

4. Conclusion

The design factors of concentric grooves, including width, depth, and pitch, were considered in this study. A CMP analysis model was developed and compared with experimental results. Several conclusions were obtained:

1. The value of the solid contact pressure is much higher than that of hydrodynamic pressure. The experimental and analytical results show that the removal rate was also dominated by the effective density of particles, which was affected by the gradient of hydrodynamic pressure variation and did not only arise from the effect of the wear depth, which was dominated by the solid contact pressure.
2. The suction hydrodynamic pressure field expands its region with increasing width and decreasing depth of grooves. The flow rate

of the slurry was thus increased, also increasing the number of abrasive particles.

3. The analytical results were consistent with the experimental results when the grooving pitch was 4 mm. The removed thickness of the silicon oxide film increased with decreasing width and depth of grooves. The optimum conditions of a concentric pad for silicon oxide polishing are a width of 1 mm, a depth of 1.2 mm, and a pitch of 4 mm for a removal rate of 3250 A/min and a non-uniformity of under 5%.

Acknowledgements

The authors would like to thank the Jui-Shin Technology Company for providing help with experimental data analyses and providing polishing pads. This study was supported by the National Science Council of Taiwan, R.O.C., under grant NSC-96-2218-E-150-003.

References

[1] F.W. Preston, The theory and design of plate glass polishing machines, J. Soc. Glass Technol. 11 (1927) 214–247.
[2] J.S. McFarlane, D. Tabor, Relation between friction and adhesion, Proc. Roy. Soc., Lond., Series A 202 (1950) 244–253.
[3] A.C. Eringen, Theory of micropolar fluids, J. Math. 16 (1966) 1–18.
[4] L.M. Cook, Chemical process in glass polishing, J. Non-Cryst. Solid 120 (1990) 152–171.
[5] S.R. Runnels, L.M. Eyman, Tribology analysis of chemical–mechanical polishing, J. Electrochem. Soc. 141 (1994) 1698–1701.
[6] S.R. Runnels, Featured-scale fluid-based erosion modeling for chemical–mechanical polishing, J. Electrochem. Soc. 141 (1994) 1900–1905.
[7] S. Sundararajan, D.G. Thakurta, D.W. Schwendeman, S.P. Murarka, W.N. Gill, Two-dimensional wafer-scale chemical–mechanical planarization models based on lubrication theory and mass transport, J. Electrochem. Soc. 146 (1999) 761–766.
[8] J. Seok, C.P. Sukam, A.T. Kim, J.A. Tichy, T.S. Cale, Multiscale material removal modeling of chemical mechanical polishing, Wear 254 (2003) 307–320.
[9] Y. Zhao, L. Chang, A. Micro-Contact, Wear model for chemical–mechanical polishing of silicon wafers, Wear 252 (2002) 220–226.
[10] T.K. Yu, C.C. Yu, M. Orlowski, A statistical polishing pad model for chemical mechanical polish, IEDM Tech. Dig. (1993) 865–868.
[11] T.K. Yu, C. Chris, M.O. Lee, Combined asperity contact and fluid flow model for chemical mechanical polishing, in: Proc. Int. Workshop on Numerical Modeling of Processes and Devices for Integrated Circuits: NUPAD V, Honolulu, HI/New York, NY, 1994, pp. 29–32.
[12] S.P. Murauka, R. Gutmann, Annual Report of the New York State Scoe, Semiconductor Research Corporation, Research Triangle Park, NC, 1994.
[13] W. Lee, D.W. Shin, M. Tomozawa, S.P. Murarka, The effect of the polishing pad treatments on the chemical mechanical polishing of SiO_2 films, Thin Solid Films 270 (1995) 601–606.
[14] J. Tichy, J.A. Levert, L. Shan, S. Danyluk, Contact mechanics and lubrication hydrodynamics of chemical mechanical polishing, J. Electrochem. Soc. 146 (1999) 1523–1528.
[15] L. Shan, J. Levert, L. Meade, J. Tichy, S. Danyluk, Interfacial fluid mechanics and pressure prediction in chemical mechanical polishing, ASME J. Tribol. 122 (2000) 539–543.
[16] J.A. Levert, S. Danyluk, J. Tichy, Mechanism for subambient interfacial pressure while polishing with liquids, ASME J. Tribol. 122 (2000) 450–457.
[17] J. Luo, D.A. Dornfeld, Material removal mechanism in chemical mechanical polishing: theory and modeling, IEEE Trans. Semicond. Manuf. 14 (2001) 112–133.
[18] Y.R. Jeng, P.Y. Huang, Impact of abrasive particles on the material removal rate in CMP, Electrochem. Solid-State Lett. 7 (2004) G40–G43.
[19] D.G. Thakurtaa, D.W. Schwendemanc, R.J. Gutmannb, S. Shankare, L. Jiange, W.N. Gill, Three-dimensional wafer-scale copper chemical mechanical planarization model, Thin Solid Films 414 (2002) 78–90.
[20] J.J. Vlassak, A model for chemical mechanical polishing of a material surface based on contact mechanics, J. Mech. Phys. Solids 52 (2004) 847–873.
[21] K. Qin, B. Moudgil, C.W. Park, A chemical mechanical polishing model incorporating both the chemical and mechanical effects, Thin Solid Films 446 (2004) 277–286.
[22] C. Wei, G. Yongjin, C. Abhijit, B. Ashraf, A scratch intersection model of material removal during chemical mechanical planarization (CMP), ASME J. Manuf. Sci. Eng. 127 (2005) 545–554.
[23] F.A. Lloy, Parameters contributing to power loss in disengaged wet clutches, SAE Technical Paper Series, 1974, Paper No. 740676.
[24] M.M. Razzzaque, T. Kato, Effects of groove orientation on hydrodynamic behaviour of wet clutch coolant films, ASME J. Tribol. 112 (1999) 409–414.
[25] E.J. Berger, F. Sadeghi, C.M. Krousgrill, Finite element modeling of engagement of rough and grooved wet clutches, ASME J. Tribol. 118 (1996) 137–146.
[26] J.F. Lin, J.D. Chern, Y.H. Chang, P.L. Kuo, M.S. Tsai, Analysis of the tribological mechanisms arising in the chemical mechanical polishing of copper-film wafers, ASME J. Tribol. 126 (2004) 185–199.
[27] J.F. Lin, S.C. Chen, Y.L. Ouyang, M.S. Tsai, Analysis of the tribological mechanisms arising in the chemical mechanical polishing of copper-film wafers when using a pad with concentric grooves, ASME J. Tribol. 128 (2006) 445–459.
[28] S.P. Timoshenko, J.N. Goodier, Theory of Elastic, McGraw-Hill, New York, 1951, pp. 1–404.
[29] D. Tabor, The Hardness of Metals, Oxford University Press, 1951.
[30] J.H. Horng, J.S. Lee, D.C. Du, Three-body microcontact model of rough surfaces and its application on polishing of wafer, Mater. Sci. Forum (2006) 507–513.
[31] Y. Xie, J.A. Wilfams, The prediction of friction and wear when a soft surface slides against a harder rough surface, Wear 196 (1996) 21–34.